An Adaptive Multi-Objective Particle Swarm Optimization Algorithm for Excitation of Focused Phased Array in Microwave Hyperthermia Treatment Planning

Si Li[1], Yifan Shen[1], Atef Z. Elsherbeni[2], Yunlong Mao[1], and Cheng Lyu[3]

[1]Ocean College
Jiangsu University of Science and Technology, Jiangsu, 212134, China
lisi0511@just.edu.cn, shenyifan@stu.just.edu.cn, maoyunlong0511@just.edu.cn

[2]Electrical Engineering Department
Colorado School of Mines, Colorado, 80401, USA
aelsherb@mines.edu

[3]Information Engineering Department
Heilongjiang Agricultural Engineering Vocational College, Heilongjiang, 150006, China
cheng666@hrbeu.edu.cn

Abstract – A novel adaptive multi-objective particle swarm optimization (AMOPSO) is proposed to address the focus shift and redundant hotspots issues prevalent in current microwave hyperthermia treatment planning for breast cancer. By optimizing the excitation of phased array elements, more accurate beam focusing effect is achieved and the redundant hotspots are reduced, which significantly improves the treatment of breast cancer. The algorithm uses the difference between the optimized and target results as a feedback to self-constrain the algorithm, and introduces ratio of the peak power absorption (pPA) between the redundant hotspots and the target hotspot as a key objective function to reduce the number of redundant hotspots. Compared with the existing hyperthermia treatment planning (HTP) optimization algorithms, the proposed algorithm is capable of achieving precise focusing and a more substantial reduction in the number of redundant hotspots in a shorter computation time. Furthermore, the introduction of the pPA is capable of more effectively reducing the number of redundant hotspots and achieving a lower damage rate to healthy tissues.

Index Terms – Hyperthermia treatment planning (HTP), particle swarm optimization (PSO), phased arrays, specific absorption rate (SAR).

I. INTRODUCTION

Breast cancer poses a serious risk to women's health and life as it is one of the most common malignant tumors in the female population [1]. Among the available technologies, microwave hyperthermia treatment (MHT) has garnered significant attention due to its distinctive advantages [2]. This technology employs phased arrays to generate focused microwaves [3], offering merits such as rapid ablation, accurate localization, ease of use, lower risk of postoperative complications, and inexpensive medical costs [4, 5].

However, the practical application of MHT remains challenging, with the most significant hurdle being the precise focalization of microwave energy on tumor tissues while avoiding damage to surrounding healthy tissues [6]. Time-reversal (TR) technique is frequently employed in the optimization of hyperthermia treatment planning (HTP). However, the focused energy usually is shifted away from the target due to the attenuation and dispersion of microwaves in biological tissues, which negatively impacts the effectiveness of the treatment. To overcome these challenges, researchers usually optimize the excitation of the phased array elements to improve the focusing performance. In order to concentrate energy in a particular area within a semicircular breast model, Curto et al. [7] used the Nelder-Mead Simplex (NMS) method to study and adjust the phase of a 4-element phased array. In another study, Elkayal et al. [8] optimized a 4-element phased array to minimize focus shift using particle swarm optimization (PSO). Although the previously described studies were successful in focusing on the tumor, the focus range was far wider than the actual tumor area, causing greater damage to the surrounding healthy tissues, and the focusing resolution was obviously insufficient.

In order to increase the resolution, increasing the number of elements of the phased array becomes an intuitive solution [9]. For example, Nguyen et al. [10]

Submitted On: June 09, 2025
Accepted On: September 18, 2025

https://doi.org/10.13052/2025.ACES.J.401002

optimized the excitation of a 24-element phased array using PSO and Lyu et al. [11] optimized an 36-element phased array using differential evolution (DE). However, while these studies improved focusing accuracy to some extent, the optimization results inevitably led to the emergence of excess hotspots in the superficial region of healthy tissues. The specific absorption rates reached 90% [10] and 115% [11] at the tumor. Although it is possible to mitigate the effects of hotspots in this part of the region using physical techniques such as cooling liquids [12], this inevitably makes the therapy procedure more complicated and expensive.

Although it is theoretically impossible to eliminate redundant hotspots due to their inherent nature in the phased array, their effects can be suppressed through optimization [13]. Traditional single-objective optimization algorithms can be limited in their effectiveness at reducing redundant hotspots. Therefore, Baskaran et al. [14] employed a multi-objective genetic algorithm (MOGA) to optimize the excitation of an 18-element phased array , achieving greater tumor coverage and fewer redundant hotspots. However, the tumor selected in this study was in the superficial layer of breast tissue, which may restrict the general applicability of the results. Moreover, MOGA suffers from slow convergence and focus shift, making it difficult to meet clinical needs.

Recent studies have indicated that prevailing optimization algorithms continue to encounter significant obstacles in attaining accurate focusing effects and effectively reducing redundant hotspots. Traditional quantitative indicators such as hotspot to target quotient (HTQ), average power absorption ratio (aPA), and specific absorption rate (SAR) are inadequate for providing a comprehensive characterization of hotspots distribution. Moreover, extant algorithms evince suboptimal efficiency and adaptability.

In this paper, an adaptive multi-objective particle swarm optimization (AMOPSO) algorithm is proposed to address these issues. First, it innovatively introduces the peak power absorption ratio (pPA) as a quantitative indicator, which provides a more comprehensive assessment of hotspot distribution features. Secondly, an adaptive feedback mechanism is designed. This mechanism adjusts key parameters, such as inertia weight and learning factor, based on the discrepancy between the optimized and target results.

The proposed AMOPSO algorithm has been demonstrated to enhance global search efficiency and environmental adaptability of the algorithm through an error feedback-based dynamic parameter adjustment strategy. The incorporation of random perturbation terms and nonlinear fitness functions serves to effectively suppress the premature convergence phenomenon of particle swarm and enhance the robustness of the algorithm. The pPA indicator, when utilized in conjunction with conventional evaluation metrics, fosters a synergistic effect, thereby facilitating the establishment of a multifaceted hotspot control evaluation system. The findings from experiments suggest that, in comparison to conventional optimization algorithms, AMOPSO demonstrates superior performance in critical metrics.

The rest of the paper is organized as follows. Section II describes the research principles of HTP, including quantitative indicators of treatment quality, the optimization algorithm, the breast model and the device. Section III presents a comparative analysis of the optimization results of this algorithm, before concluding with a summary in section IV.

II. THE PROPOSED ALGORITHM

A. Quantitative indicators of treatment quality

The aim of HTP is to accurately concentrate electromagnetic wave energy within the tumor, while preventing the formation of redundant hotspots in healthy tissue. If total thermal damage to the tumor tissue can be accomplished and thermal damage to the surrounding healthy tissue is kept to less than 5%, the HTP is usually regarded as safe and successful [15].

The energy density deposition $Q(r)$ in the breast tissue is expressed as

$$Q(r) = 0.5\sigma(r)|\vec{E}(r)|^2, \tag{1}$$

where $r = (x, y, z)$ are spatial coordinates, $\sigma(r)$ is the conductivity of the tissue and $\vec{E}(r)$ is the total electric field inside the tissue, which is given by

$$\vec{E}(r) = \sum_{i=0}^{N-1} A_I e^{-i\varphi_i} \vec{E}_i(r), \tag{2}$$

where A_i and φ_i are the amplitude and phase delays of the ith antenna element, $\vec{E}_i(r)$ is the electric field provided by the ith antenna, and N ($N = 16$ in this work) is the number of antenna elements in the phased array. Normally, we use SAR as a measure of absorbed electromagnetic energy per unit time per unit mass of a biological tissue [16], in units of W/kg. $SAR(r)$ is expressed as

$$SAR(r) = \frac{Q(r)}{2\rho(r)} = \frac{\sigma(r)|\vec{E}(r)|^2}{2\rho(r)}, \tag{3}$$

where $\rho(r)$ is the density of the tissue. Since the physical properties of breast tissue are incorporated into the SAR calculation, the absorption of electromagnetic wave energy by breast tissue can be accurately observed through the SAR distribution.

When building the HTP optimization model, the focus shift and the number of hotspots are usually taken as the main optimization targets to ensure the precision and safety of the treatment effect, weighing up treatment accuracy and energy distribution uniformity. At the same time, the model must consider several key indicators comprehensively: HTQ, aPA, tumor coverage n% (TC_n) and damaged healthy tissue rate (DHTR) to enhance the therapeutic effect and minimize damage to normal tissues [17].

The focal shift is the spatial distance between the center of the region of strongest energy focus and the center of the target tumor, which is given by

$$FS = \|r_c - r_t\|_2, \tag{4}$$

where $r_t = (x_t, y_t, z_t)$ is the center coordinates of the tumor, $r_c = (x_c, y_c, z_c)$ is the center coordinates of the strongest hotspot, obtained by

$$r_c = \frac{1}{n(H_c)} \sum_{r \in H_c} r, \tag{5}$$

where

$$H_c = \{r \in H_{\max} \mid SAR(r) \geq 0.9 \times \max(SAR(r))\}, \tag{6}$$

$n(H_c)$ is the total number of points belonging to the center area H_c of the strongest hotspot $H_{\max}$, which is expressed as

$$H_{\max} = \arg\max_{H_i} \left(\max_{r \in H_i} SAR(r) \right), \tag{7}$$

$$H_i = \left\{ r \mid SAR(r) \geq \frac{1}{\sqrt{2}} \times \max(SAR(r)) \right\}, \tag{8}$$

H_i is the region of hotspots, and the strongest one is $H_{\max}$. The total number of H_i is the number of hotspots N.

HTQ assesses the relationship between the region of highest energy intensity and the average energy of the tumor. It is expressed as the ratio of average SAR values between in the top 1% healthy tissues and in the tumor, which is

$$HTQ = \overline{SAR}_{V_1} / \overline{SAR}_t, \tag{9}$$

where V_1 is the volume of the top 1% of healthy tissues with SAR values ranking from the highest to the lowest, $\overline{SAR}_{V_1}$ and $\overline{SAR}_t$ are the average SAR value in V_1 and in the tumor.

aPA assesses the relative energy absorbed by tumors. It is calculated by expressing the average energy difference between tumor tissue and healthy tissue, which is

$$aPA = \frac{(\sum P_t)/V_t}{(\sum P_h)/V_h}, \tag{10}$$

where P_t and P_h denote the power absorbed by the tumor and healthy tissue, respectively, V_t and V_h are the volumes of the tumor and healthy tissue, respectively.

TC_n is expressed as

$$TC_n = V_i(SAR > \max(SAR) \times n\%)/V_i, \tag{11}$$

TC_n represents the percentage of tumor volume in which the SAR value exceeds n% of the highest SAR observed within the tumor.

DHTR was calculated using the formula

$$DHTR = V_d/V_n, \tag{12}$$

where V_n is the volume of healthy tissue within 15 mm from the tumor edge, V_d is the volume of damaged healthy tissues.

However, the assessment of HTQ and aPA can vary significantly for different array sizes and breast models. This variability poses challenges in standardizing evaluation criteria and identifying redundant hotspots. When these indicators are used as the objective functions in algorithms, they often fail to effectively reduce redundant hotspots, thereby increasing computational complexity and optimization difficulty. To address these limitations, this study proposes a novel indicator, the pPA, which enables a comprehensive analysis of SAR distribution characteristics and hotspot distribution, particularly the relationship between the strongest absorption region and other high-absorption areas.

The pPA can be obtained through an analytical method based on the correlation of SAR values with their respective domains. The fundamental aspect of the method is the identification and determination of local peaks and locations of SAR values within the tissue by establishing a link between a specific point of interest and its corresponding domain. Subsequently, the strongest peak among these identified peaks is taken to be the main hotspot, whose SAR value is $SAR_{peakmax}$. The maximum value after comparing the SAR value $SAR_{peak}(i)$ at the remaining peak points with the SAR value $SAR_{peakmax}$ at the main hotspot is defined as the pPA, which is expressed as

$$pPA = \max\left(\frac{SAR_{peak}(i)}{SAR_{peakmax}} \right). \tag{13}$$

In comparison with existing indicators, pPA directly quantifies the relative strength of secondary hotspots compared to main hotspot, thereby providing higher accuracy in hotspot characterization. Furthermore, it possesses a discernible threshold for hotspot redundancy: when pPA is less than $1/\sqrt{2}$, SAR distribution guarantees that there is only one valid hotspot [18, 19], accurately quantifying the optimization objective.

B. The proposed algorithm

In the PSO, a population of N particles searches in a space of dimension D. At the tth iteration, the vectors of position $X_{i,t}$ and velocity $V_{i,t}$ of each individual $i(1 \le i \le N)$ in the population are represented by $X_{i,t}^j = (X_{i,t}^1, X_{i,t}^2, \ldots, X_{i,t}^D)$ and $V_{i,t}^j = (V_{i,t}^1, V_{i,t}^2, \ldots, V_{i,t}^D)$, respectively. Each iteration updates the velocity and position of each particle in each dimensional component on the basis of the found locally optimal solution and the globally optimal solution , which is updated as

$$V_{i,t+1}^j = wV_{i,t}^j + c_1 \mathrm{r}_{i,n}^j (P_{i,t}^j - X_{i,t}^j) + c_2 \mathrm{R}_{i,t}^l (G_{i,t}^j - X_{i,t}^j), \tag{14}$$

$$X_{i,t+1}^j = X_{i,t}^j + V_{i,t+1}^j, \tag{15}$$

where $i = 1,2,\ldots,N$, $j = 1,2,\ldots,D$, w is the inertia weight, c_1 and c_2 are the learning factors, $\mathrm{r}_{i,n}^j$ and $\mathrm{R}_{i,n}^j$ are two random numbers uniformly distributed in the range [0,1].

In the context of multi-objective optimization scenarios, existing multi-objective PSO algorithms encounter several limitations when they are extended [20–23]. Firstly, their adaptive strategies are devoid of a robust theoretical foundation, exhibiting an inadequate examination of particle movement characteristics and predominantly relying on a singular search strategy for updating particle states. Secondly, these algorithms neglect to consider the disparities in the optimization capabilities of individual particles, which hinders the achievement of a balance between algorithm convergence and solution diversity when confronted with complex optimization problems. Finally, the switching mechanism between global exploration and local exploitation remains imperfect, causing the algorithms to easily fall into local optimal solutions or suffer from insufficient convergence accuracy.

In order to enable the algorithm to dynamically adjust the balance between local and global searches according to the optimization effect, this paper proposes an adaptive search method combining a feedback adjustment mechanism and a random perturbation strategy. This method uses the discrepancy between the optimized and targeted results as a feedback signal to adaptively adjust the inertia weights and learning factors. The complete flowchart of the algorithm is shown in Fig. 1.

The adaptive functions of each parameter are

$$w(x) = 0.65 + 0.5 \times \cos\left(\frac{\pi}{2\sqrt{x}} + \frac{\pi}{3}\right) + \left(0.5 - 0.1 \times \cos\left(\frac{\pi}{2x}\right)\right) \times r, \tag{16}$$

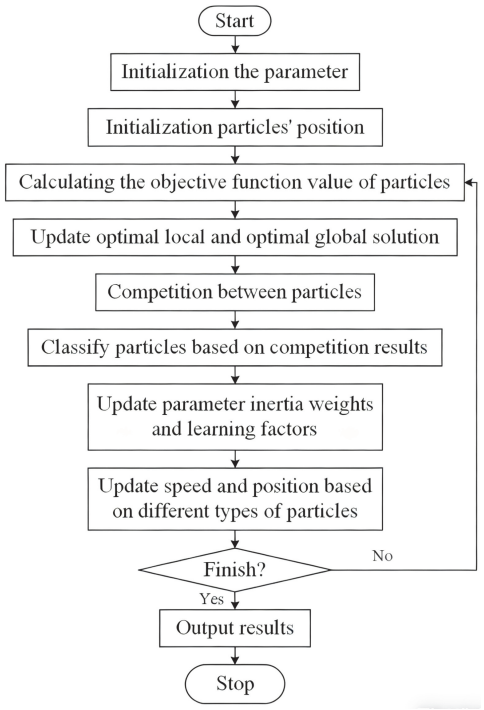

Fig. 1. Flowchart of the AMOPSO algorithm.

$$c_1(x) = 1.6 - 0.4 \times \sin\left(\frac{\pi}{2x}\right) + \left(0.4 - 0.2 \times \cos\left(\frac{\pi}{2x}\right)\right) \times r, \tag{17}$$

$$c_2(x) = 1.4 + 0.4 \times \sin\left(\frac{\pi}{2x}\right) + \left(0.4 - 0.2 \times \cos\left(\frac{\pi}{2x}\right)\right) \times r, \tag{18}$$

where $x = \sum a_i \cdot (opt_i - tar_i)(x > 0)$ is the fitness function related to the target parameters tar_i of the optimization process, a_i is defined as the weight corresponding to the optimized results opt_i, which is influenced by the importance of the ith target result, the range of variation and the optimization process.

The configuration of the parameters is illustrated in Fig. 2. As shown in the figure, it depicts the corresponding values of parameters w, c_1, and c_2 when the fitness function x takes values within the range of [0,20]. Considering the presence of random functions in (16), (17) and (18), the simulation interval is set to 0.01.

The formula is composed of three primary components: a constant term, a trigonometric term, and a random perturbation term. The constant term is established in accordance with the empirical ranges of the inertia weight and learning factor from traditional PSO [20, 21], thereby ensuring that the algorithm maintains its optimization capability during local exploitation. In contrast to the parameter changes observed in conventional

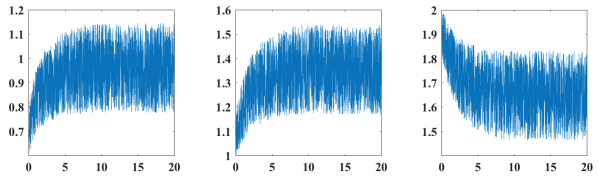

Fig. 2. Parameter configuration simulation diagram. (a) w, (b) c_1, (c) c_2.

AMOPSO, the trigonometric function term establishes a dynamic adjustment mechanism based on a nonlinear function. It considers the parameter intervals and transition criteria for the global exploration and local exploitation phases, accurately reflecting the dynamic changes in optimization. This nonlinear adaptation enhances global search, thereby preventing premature convergence and ensuring a balance between exploration and exploitation. The random perturbation term employs the random variable r to augment the algorithm's robustness, thereby substantially enhancing population diversity while preserving convergence efficiency. Compared to existing mainstream AMOPSO algorithm, this method demonstrates superior problem adaptability and maintains stable and reliable optimization performance in complex noisy environments and dynamic scenarios.

Furthermore, in order to optimize the utilization of the resources of each individual particle, the velocity is reassigned to those particles that have been identified as outliers over an extended period of time. This enables them to rapidly exit the outlier state. The particle velocity reset function V_r is

$$V_r^j = \frac{a_{FS}}{1+\exp\left(-\left(\Delta FS-5\right)/1.5\right)} + \frac{a_{pPA}}{1+\exp\left(-2\times\Delta pPA\right)} - a, \tag{19}$$

where a_{FS}, a_{pPA} and a are constants. $\Delta FS = FS_{best} - FS_{target}$, FS_{best} and FS_{target} are the optimal and target values of the focus shift. $\Delta pPA = pPA_{best} - pPA_{target}$, pPA_{best} and pPA_{target} are the optimal and target values of pPA, V_r^j is the velocity vector of the newborn particle, which decreases gradually with the optimization process, allowing the search range to shrink gradually to improve accuracy. In comparison with the rudimentary approach employed in existing AMOPSO algorithms [20, 24], the velocity reset strategy, which takes into account the discrepancies between optimized and targeted results, demonstrates superior performance. The system has been demonstrated to adaptively reset velocities for outliers, thereby boosting swarm activity and guiding them back to the search path. This, in turn, accelerates optimization and enhances accuracy.

C. Breast model and phased array device

The phased array model for MTP by the global optimization algorithm is shown in Figs. 3 (a) and (b).

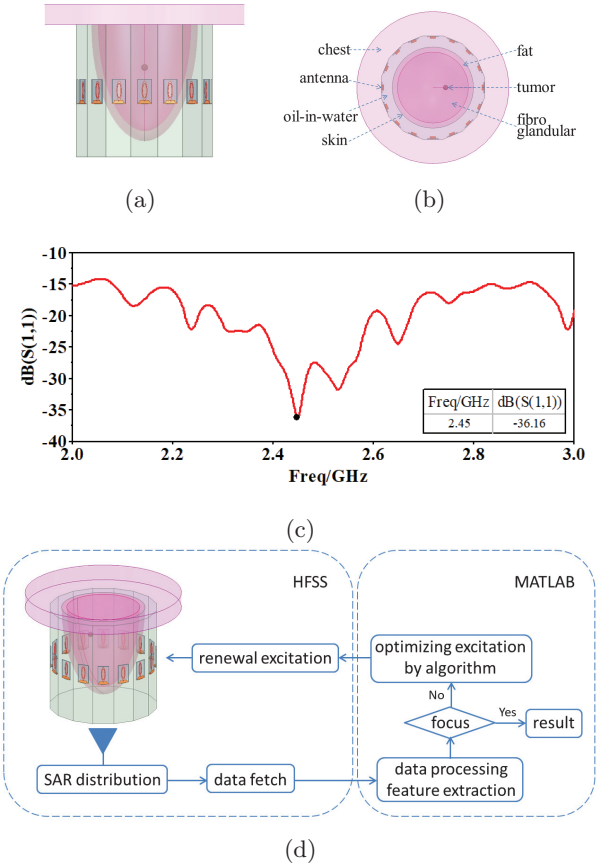

Fig. 3. Optimization process of phased array excitation in HTP: (a) side view, (b) top view, (c) S_{11} parameters of the phased array element, (d) flowchart of HTP.

The simplified breast model is placed in a circular phased array formed by 16 antenna elements uniformly aligned with a radius of 100 mm and a height of 200 mm. The size of the phased array element is 31.25 mm $\times$ 21.4 mm, and it is made of Rogers RT5880 with dielectric constant of 2.2, loss angle tangent of 0.009, and thickness of 1.575 mm. S_{11} parameter is shown in Fig. 3 (c), which is in working condition with $S_{11} < -10$ dB at 2–3 GHz and achieves a good performance of -36 dB at the operating frequency of 2.45 GHz. The phased array and breast model were immersed in a coupling fluid (oil-in-water) with a relative dielectric constant of 22.9 and a conductivity of 0.07. The breast model consisted of skin, fat, breast fibers, and tumor [25].The HTP optimization process is shown in Fig. 3 (d). SAR distribution data can be obtained by HFSS simulation and then processed and analyzed to obtain the previously mentioned indicators in Matlab. The excitation of

the phased array is iteratively optimized and adjusted according to these indicators until it meets the predefined objectives. Finally, we can obtain the appropriate excitations of elements.

III. RESULTS AND ANALYSIS

A. Experimental results of different optimization algorithms

In order to demonstrate the performance advantages of the proposed AMOPSO algorithm, we compare it with linearly decreasing weights PSO (LDW-PSO) [26], GA [14], DE [11] and an adaptive MOPSO with multi-strategy based on energy conversion and explosive mutation (ecemAMOPSO) [20]. In the course of the comparison experiments, the algorithms were configured to utilize the same population size, objective function, number of iterations, and initial values. The simulations and optimization procedures were applied to tumors located at (0, 35, 35) mm.

The normalized SAR distributions of the optimization effects of different optimization algorithms focusing are shown in Fig. 4. The experimental simulation results are shown in the breast model to observe the SAR distribution more clearly. The red object represents the tumor, and the rectangle represents the simplified antenna structure. The axial and coronal planes are selected based on the location of the tumor center. The normalized SAR distribution is shown in the plan view, and the positions corresponding to the 3D map are marked. It can also be observed that the AMOPSO algorithm achieved accurate focusing and effectively reduced redundant hotspots, and there were no redundant hotspots in the region outside the focal plane of interest.

Table 1 shows the optimization results of each algorithm. As observed, the LDW-PSO algorithm still has difficulty in finding a desirable balance in multi-objective optimization despite its improved weighting strategy. The DE algorithm is unable to achieve synergistic optimization among multiple objectives despite its strong global search capability, thus affecting the overall performance.

Table 1: Quantitative indicators of treatment quality with different algorithms

	FS	**n**	**pPA**	**aPA**	**HTQ**	**TC_{70}**	**DHTR**
DE	1.90	13	0.86	4.22	0.86	96.13%	18.48%
LDW-PSO	1.91	3	0.78	4.62	0.70	94.36%	12.50%
GA	0.36	4	0.71	5.28	0.75	98.91%	9.94%
ecem-AMO-PSO	0.30	3	0.75	5.90	0.75	99.80%	7.77%
AMO-PSO	0.32	1	0.46	5.95	0.64	99.97%	4.53%

While both the GA and ecemAMOPSO algorithms have been demonstrated to achieve high precision in identifying the optimization target, the GA algorithm's capacity for local development is comparatively deficient. This limitation impedes the effective removal of redundant hotspots. The adjustment process of the parameter in ecemAMOPSO is closely coupled with the duration of the iteration, which makes it difficult for the algorithm to achieve stable convergence in a limited time, resulting in redundant hotspots remaining outside the target observation plane. In contrast, the AMOPSO algorithm is significantly superior to other algorithms in all indicators of pPA, HTQ, aPA and DHTR, which proves the excellent comprehensive optimization ability of AMOPSO high precision and multiple objectives.

The excitation results of the phased array obtained after optimization using the AMOPSO algorithm are presented in Table 2. The phase is defined as the relative phase difference with respect to element 1, with a range of $[-180^\circ, 180^\circ]$, and the amplitude is the feeding coefficient, with a range of [0, 1].

Table 2: Excitation of phased array elements

Element Number	**1**	**2**	**3**	**4**
phase(°)	0	39.57	−163.06	38.11
amplitude	1	1	0.78	0.80
Element Number	**5**	**6**	**7**	**8**
phase(°)	−75.19	−157.14	−91.41	−101.58
amplitude	0.59	1	0.82	1
Element Number	**9**	**10**	**11**	**12**
phase(°)	172.56	45.34	−48.15	−160.15
amplitude	0.34	1	1	1
Element Number	**13**	**14**	**15**	**16**
phase(°)	−64.71	49.60	−150.99	42.44
amplitude	0.37	0.97	0.82	1

In the context of microwave hyperthermia treatment plans, the presence of phased array phase errors has been observed to exert an influence on the performance indicators associated with treatment outcomes. A systematic investigation was conducted to evaluate the performance of phased array MHT under specific phase error conditions. To this end, 50 independent replicate experiments were performed, with phase differences fluctuating within a range of $\pm 10^\circ$ [27]. The maximum (Max), minimum (Min), average (Ave), and standard deviation (SD) of the experimental results are shown in Table 3.

The experimental results show that changes in phase difference parameters significantly affect the accuracy of focus positioning. This results in the FS and DHTR exceeding the established limit. While certain indicators may exceed the established limits, statistical analysis reveals that such deviations are not pervasive, and the results persist within acceptable ranges. The majority

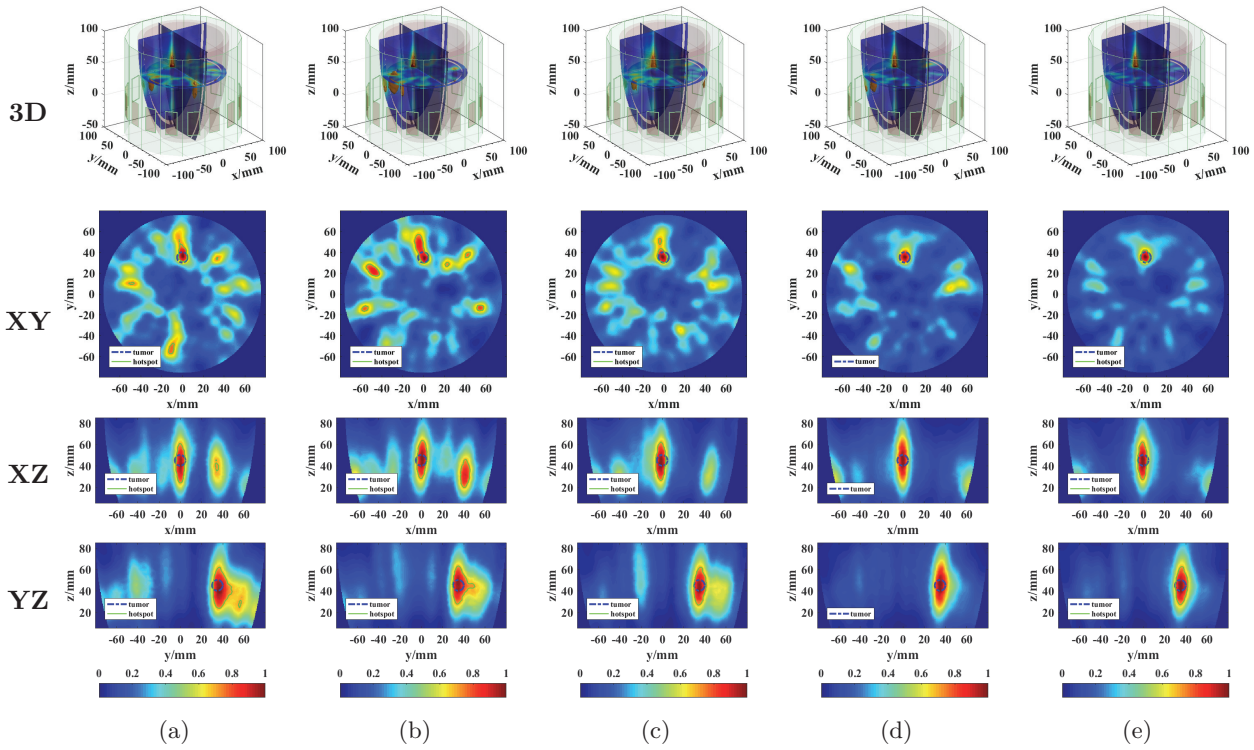

Fig. 4. Normalized SAR distribution with different algorithms. (a) DE, (b) LDW-PSO, (c) GA, (d) ecemAMOPSO, (e) AMOPSO.

Table 3: The impact of phase error on optimization results

	FS	n	pPA	aPA	HTQ	TC_{70}	DHTR
Max	0.526	1	0.653	6.071	0.675	99.951%	5.153%
Min	0.311	1	0.421	5.854	0.639	98.594%	4.297%
Ave	0.373	1	0.522	5.537	0.642	99.873%	4.581%
SD	0.081	1	0.053	0.056	0.006	0.419	0.249

of indicators meet the specified requirements, thereby demonstrating that the phased array system in MHTP exhibits a certain degree of stability and reliability under most conditions.

In consideration of the correlation between the diversity of breast tissues and the efficacy of MHT, this study employs the dielectric constant of breast tissues as the primary variable for experimental analysis [28]. This study systematically investigated the impact of dielectric constant fluctuations within a range of $\pm 10\%$ on key quantitative indicators for thermotherapy. The experimental results are shown in Table 3.

The experimental data demonstrate that alterations in the dielectric constant of the tissue result in variability among all performance indicators of the system. However, it is observed that all indicators meet the established requirements, and the impact is deemed to be within acceptable limits.

Table 4: The impact of dielectric constant fluctuations on optimization results

	FS	n	pPA	aPA	HTQ	TC_{70}	DHTR
Max	0.450	1	0.618	5,962	0.697	99.841%	4.893%
Min	0.320	1	0.445	5.642	0.640	96.714%	4.531%

B. Experimental results of algorithms optimized for tumors at different locations

Due to the intricate distribution of dielectric properties, the difficulty of performing HTP varies for tumors at different locations and depths. To verify that the algorithm proposed can achieve optimal treatment for a wide range of tumors, we performed focused experiments using the AMOPSO algorithm for tumors located at (0, 25, 50) mm, (0, 35, 35) mm, (0, 45, 45) mm and (0, 55, 30) mm, respectively.

The normalized SAR distributions of tumors at different positions are shown in Fig. 5.

As the location of the tumor deepens, electromagnetic waves are more scattered and absorbed when penetrating tissues, which causes the electromagnetic wave energy to be more dispersed and decay more rapidly. It can be observed from Fig. 5 that, as the tumor approaches the mid-axis of the breast tissue, the focal length progressively increases. Simultaneously,

the energy peak outside the focal region slightly rises, and the focal area gradually elongates. This phenomenon can be attributed to the scattering effect experienced by the electromagnetic waves as they penetrate the tissue, leading to a more dispersed energy distribution and thus an elongated focal region. Additionally, the absorption of electromagnetic wave energy by the breast tissue accelerates the attenuation of the waves, causing the focal region to become narrower. This attenuation not only alters the shape of the hotspot but also impacts on the overall efficacy of the treatment.

The results of the focus optimization process for tumors at different locations are presented in Table 5. The DHTR value was found to be less than 5% for all locations that were examined, suggesting that there was minimal damage to healthy tissues. The lowest pPA was observed at the focal position (0,45,40) mm. It is important to note that the aPA exhibited a gradual decrease in trend as the position of the tumor progressed deeper into the breast tissue. This finding suggests a strong correlation between the energy absorption efficiency and the spatial distribution of the focal point.

Table 5: Quantitative indicators of treatment quality optimized at different locations using AMOPSO

	FS	**n**	**pPA**	**aPA**	**HTQ**	**TC_{70}**	**DHTR**
(0,25,50)	0.48	1	0.64	5.08	0.71	96.20%	3.78%
(0,35,35)	0.32	1	0.46	5.95	0.64	99.30%	4.54%
(0,45,45)	0.46	1	0.36	7.88	0.69	99.70%	4.75%
(0,55,30)	0.33	1	0.45	8.46	0.62	100%	4.80%

C. Experimental results for different objective functions in AMOPSO

The AMOPSO algorithm is a system that guides the movement of an individual based on the discrepancy between optimized and target results. The objective function affects the optimization performance of the algorithm. In order to verify the applicability and superiority of the proposed objective function in HTP applications, an experimental comparative analysis was conducted to explore the optimization effect of different objective functions. The minimization objectives that have been selected for the optimization of the treatment of tumors located at (0, 35, 35) mm are as follows

$$\min(FS, 1/aPA), \tag{20}$$

$$\min(FS, HTQ), \tag{21}$$

$$\min(FS, pPA, 1/aPA, HTQ). \tag{22}$$

The optimized normalized SAR distribution is shown in Fig.6. It is evident from Fig. 6 that the outcomes obtained using the three optimization objectives are devoid of focus shift and redundant hotspot problems, thereby substantiating the AMOPSO algorithm's robust generalization capability.

The optimization results for each objective are displayed in Table 6. In the instance of objective (20) being utilized as the optimization objective, the value of aPA was determined to be 33.35% and 33.01% higher compared to objective (21) and (22), respectively. This optimization objective intuitively reflects the difference in energy absorption levels in the region of tumor and healthy tissues, achieved by decreasing the mean energy of the healthy tissue and increasing the mean energy of the tumor tissue. This results in an optimization that exhibits enhanced energy coverage within the region of tumor, though concomitantly results in elevated levels of healthy tissue damage.

Table 6: Quantitative indicators of treatment quality using AMOPSO with different objectives

	FS	**n**	**pPA**	**aPA**	**HTQ**	**TC_{70}**	**DHTR**
Obj.(20)	0.33	1	0.63	0.68	7.91	100%	5.08%
Obj.(21)	0.33	1	0.49	0.66	5.93	99.70%	5.30%
Obj.(22)	0.32	1	0.46	5.95	0.64	99.30%	4.54%

In the instance of objective (21) being utilized as the optimization objective, the value of HTQ was found to be 3.36% lower in comparison to objective (20), yet 3.15% higher than objective (22). The function of objective (21) is to reduce the average energy of healthy tissue, thereby reducing the energy in the tumor. This results in an enhancement of the contrast between the average energy of the tumor and the energy of the region of highest energy intensity within the healthy tissue. However, this adjustment resulted in the facile dispersion of energy to other regions of the tissue, giving rise to aPA values that were 35.01% and 0.23% lower than the values observed for the other two objectives. This resulted in a reduction in energy utilization and an increase in TC_{70}, as well as a decrease in DHTR, in comparison to the other two objectives.

In the instance of objective (22) being utilized as the optimization objective, the indicator of pPA effectively evaluates the distribution of the strongest hotspot and other important hotspots, thus demonstrating the most comprehensive optimization effect. The value of pPA is reduced by 25.8% and 6.1%, and the value of DHTR is reduced by 10.8% and 14.6%, respectively, compared with the other two objectives. It is evident that this has led to a substantial enhancement in the degree of optimization, which has consequently resulted in a notable reduction in the damage caused to healthy tissue, alongside a significant increase in the concentration of microwave energy. This finding suggests that the AOMPSO algorithm, utilizing objective (22) as the

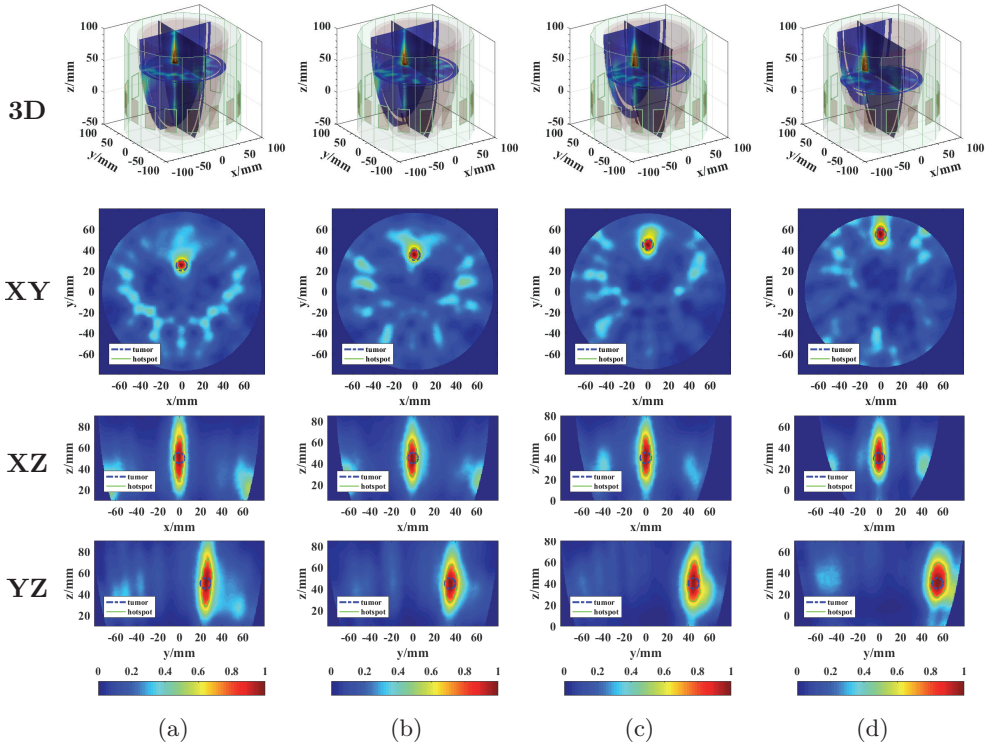

Fig. 5. Normalized SAR distribution with tumors at different locations using AMOPSO. (a) (0,25,50) mm, (b) (0,35,35) mm, (c) (0,45,45) mm, (d) (0,55,30) mm.

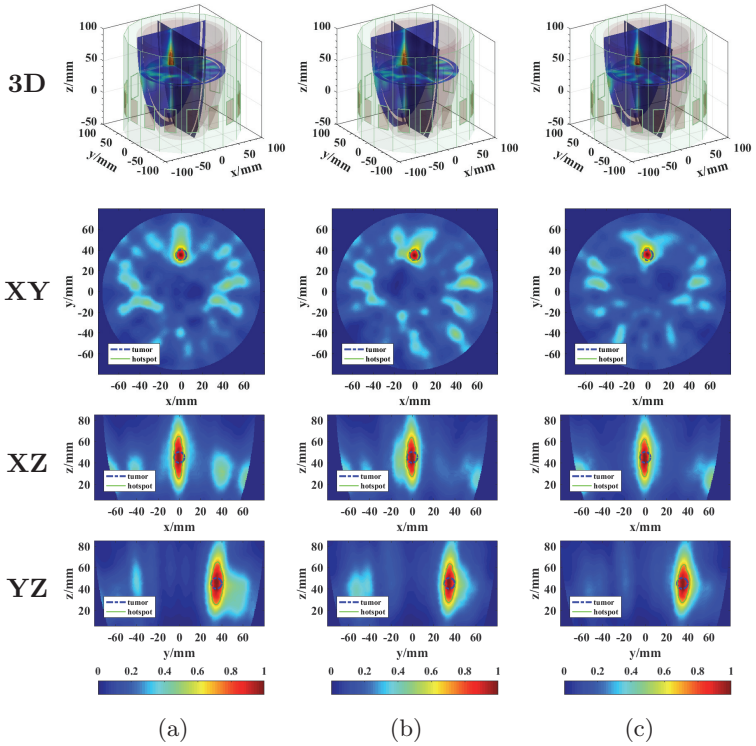

Fig. 6. Normalized SAR distribution with different objectives. (a) Obj.(20), (b) Obj.(21), (c) Obj.(22).

objective, is most effective in the context of phased array microwave hyperthermia treatment for breast cancer. This not only enhances the efficacy of treatment but also ensures the minimization of energy distribution and tissue damage in healthy tissues.

IV. CONCLUSION

In this paper, an AMOPSO algorithm is introduced as a groundbreaking solution to address the problems of focus shift and redundant hotspots in the HTP process of breast cancer. What sets the AMOPSO algorithm apart is its unparalleled superiority, as evidenced by comprehensive comparative analyses against other optimization algorithms. It not only outperforms its counterparts in terms of optimization efficacy but also stands out with its remarkable efficiency. This rapid convergence enables the algorithm to achieve pinpoint focusing accuracy while drastically reducing the number of redundant hotspots, resulting in a significantly enhanced treatment outcome for tumors.

One of the AMOPSO algorithm's most distinctive features is its exceptional adaptability to different tumor locations. An exhaustive investigation into its focalizing aptitudes reveals that the algorithm reliably attains predetermined objectives with exactitude, notwithstanding the intensifying complexity associated with more profound tumor locations. This showcases its remarkable ability to maintain accurate focusing over a wide range of scenarios, highlighting its broad applicability and versatility, which far surpasses that of many existing algorithms.

Additionally, the paper meticulously compares different SAR-based objective functions and uncovers a unique advantage of the AMOPSO algorithm. By incorporating pPA as an objective function, the algorithm substantially improves treatment effectiveness, outperforming traditional objective functions commonly used in HTP. This innovative approach represents a significant advancement in the field and demonstrates the AMOPSO algorithm's potential to redefine microwave thermal therapy optimization standards.

REFERENCES

[1] Y. Xu, M. Gong, Y. Wang, Y. Yang, S. Liu, and Q. Zeng, "Global trends and forecasts of breast cancer incidence and deaths," *Scientific Data*, vol. 10, no. 1, p. 334, May 2023.

[2] W. Zhu, S. Pan, J. Zhang, J. Xu, R. Zhang, Y. Zhang, Z. Fu, Y. Wang, C. Hu, and Z. Xu, "The role of hyperthermia in the treatment of tumor," *Critical Reviews in Oncology/Hematology*, vol. 204, p. 104541, Dec. 2024.

[3] A. Westra and W. Dewey, "Variation in sensitivity to heat shock during the cell-cycle of Chinese hamster cells in vitro," *International Journal of Radiation Biology and Related Studies in Physics, Chemistry and Medicine*, vol. 19, no. 5, pp. 467–477, Jan. 1971.

[4] X. Chen, L. Tan, T. Liu, and X. Meng, "Micro-nanomaterials for tumor microwave hyperthermia: Design, preparation, and application," *Current Drug Delivery*, vol. 14, no. 3, pp. 307–322, Apr. 2017.

[5] C. G. Pang, Z. F. Huang, S. L. Ji, H. Zhang, Y. L. Zhao, and Y. C. Hu, "Microwave-induced hyperthermia in situ in the treatment of tumors of proximal humerus: Long-term results with functionary sparing surgery," *Journal of Orthopaedic Surgery and Research*, vol. 18, no. 1, p. 433, June 2023.

[6] M. T. Bevacqua, R. Gaffoglio, G. G. Bellizzi, M. Righero, G. Giordanengo, L. Crocco, G. Vecchi, and T. Isernia, "Field and temperature shaping for microwave hyperthermia: Recent treatment planning tools to enhance SAR-based procedures," *Cancers*, vol. 15, no. 5, p. 1560, Mar. 2023.

[7] S. Curto, A. Garcia-Miquel, M. Suh, N. Vidal, J. M. Lopez-Villegas, and P. Prakash, "Design and characterisation of a phased antenna array for intact breast hyperthermia," *International Journal of Hyperthermia*, vol. 34, no. 3, pp. 250–260, Apr. 2018.

[8] H. A. Elkayal and N. E. Ismail, "Efficient focusing of microwave hyperthermia for small deep-seated breast tumors treatment using particle swarm optimization," *Computer Methods in Biomechanics and Biomedical Engineering*, vol. 24, no. 9, pp. 985–994, July 2021.

[9] X. Tang, X. Qing, N. Nasimuddin, Y. Zhou, B. Luo, W. Wang, and F. Chin, "Beam steering resolution for large antenna array," in *2021 IEEE International Symposium on Antennas and Propagation and USNC-URSI Radio Science Meeting (APS/URSI)*, pp. 273–274, IEEE, Singapore, Singapore, Dec. 2021.

[10] P. T. Nguyen, A. Abbosh, and S. Crozier, "Three-dimensional microwave hyperthermia for breast cancer treatment in a realistic environment using particle swarm optimization," *IEEE Transactions on Biomedical Engineering*, vol. 64, no. 6, pp. 1335–1344, June 2017.

[11] C. Lyu, W. Li, and B. Yang, "Differential evolution optimization of microwave focused hyperthermia phased array excitation for targeted breast cancer heating," *Sensors*, vol. 23, no. 8, p. 3799, Apr. 2023.

[12] M. Converse, E. Bond, B. Veen, and C. Hagness, "A computational study of ultra-wideband versus narrowband microwave hyperthermia for breast cancer treatment," *IEEE Transactions on Microwave Theory and Techniques*, vol. 54, no. 5, pp. 2169–2180, May 2006.

[13] Y. Zhang, Z. Han, S. Tang, S. Shen, C.-Y. Chiu, and R. Murch, "A highly pattern-reconfigurable

planar antenna with 360Â° single- and multi-beam steering," *IEEE Transactions on Antennas and Propagation*, vol. 70, no. 8, pp. 6490–6504, Aug. 2022.

[14] D. Baskaran and K. Arunachalam, "Multiobjective optimization of microwave phased array excitation for targeted tissue heating with reduced channel power in hyperthermia treatment planning," *IEEE Transactions on Microwave Theory and Techniques*, vol. 70, no. 1, pp. 622–630, Jan. 2022.

[15] O. Kivekäs, T. Lehtiniemi, and P. Vainikainen, "On the general energy-absorption mechanism in the human tissue," *Microwave and Optical Technology Letters*, vol. 43, no. 3, pp. 195–201, Nov. 2004.

[16] H. P. Kok, G. Schooneveldt, A. Bakker, R. De Kroon-Oldenhof, L. Korshuize-van Straten, C. E. De Jong, E. Steggerda-Carvalho, E. D. Geijsen, L. J. A. Stalpers, and J. Crezee, "Predictive value of simulated SAR and temperature for changes in measured temperature after phase-amplitude steering during locoregional hyperthermia treatments," *International Journal of Hyperthermia*, vol. 35, no. 1, pp. 330–339, Dec. 2018.

[17] Z. Xi, X. Wang, K. Ye, and X. Wang, "Performance evaluation of focused microwave brain hyperthermia guided by microwave-induced thermoacoustic tomography," *IEEE Journal of Electromagnetics, RF and Microwaves in Medicine and Biology*, vol. 7, no. 4, pp. 383–391, Dec. 2023.

[18] A. Buffi, P. Nepa, and G. Manara, "Design criteria for near-field-focused planar arrays," *IEEE Antennas and Propagation Magazine*, vol. 54, no. 1, pp. 40–50, Feb. 2012.

[19] Q. Liang, B. Chen, H. Wu, C. Ma, and S. Li, "A novel modified sparrow search algorithm with application in side lobe level reduction of linear antenna array," *Wireless Communications and Mobile Computing*, vol. 2021, no. 1, p. 9915420, Jan. 2021.

[20] W. Huang and W. Zhang, "Adaptive multi-objective particle swarm optimization with multi-strategy based on energy conversion and explosive mutation," *Applied Soft Computing*, vol. 113, p. 107937, Dec. 2021.

[21] Q. Gu, M. Jiang, S. Jiang, and L. Chen, "Multi-objective particle swarm optimization with R2 indicator and adaptive method," *Complex & Intelligent Systems*, vol. 7, no. 5, pp. 2697–2710, Oct. 2021.

[22] M. Mansouri, H. R. Safavi, and F. Rezaei, "An improved MOPSO algorithm for multi-objective optimization of reservoir operation under climate change," *Environmental Monitoring and Assessment*, vol. 194, no. 4, p. 261, Mar. 2022.

[23] J. Gong, H. Li, H. Yu, L. Shu, Z. Zhang, X. Han, and W. Lun, "Optimization of multi-pass coating for magnetic-thermal-assisted laser cladding based on data-enhanced WOA-DE-TELM and LHS-AMOPSO algorithm," *Surface and Coatings Technology*, vol. 497, p. 131765, Feb. 2025.

[24] G. Y. Yi, M. J. Kim, H. I. Kim, J. Park, and S. H. Baek, "Hyperthermia treatment as a promising anti-cancer strategy: Therapeutic targets, perspective mechanisms and synergistic combinations in experimental approaches," *Antioxidants*, vol. 11, no. 4, p. 625, Mar. 2022.

[25] C. Lyu, W. Li, S. Li, Y. Mao, and B. Yang, "Design of ultra-wideband phased array applicator for breast cancer hyperthermia therapy," *Sensors*, vol. 23, no. 3, p. 1051, Jan. 2023.

[26] H. Liu, X.-W. Zhang, and L.-P. Tu, "A modified particle swarm optimization using adaptive strategy," *Expert Systems with Applications*, vol. 152, p. 113353, Aug. 2020.

[27] G. He, X. Gao, and R. Zhang, "Impact analysis and calibration methods of excitation errors for phased array antennas," *IEEE Access*, vol. 9, pp. 59010–59026, 2021.

[28] A. Martellosio, M. Pasian, M. Bozzi, L. Perregrini, A. Mazzanti, F. Svelto, P. E. Summers, G. Renne, L. Preda, and M. Bellomi, "Dielectric properties characterization from 0.5 to 50 GHz of breast cancer tissues," *IEEE Transactions on Microwave Theory and Techniques*, vol. 65, no. 3, pp. 998–1011, Mar. 2017.

Si Li was born in Harbin, Heilongjiang, China, in 1987. She received the B.S. degree in electrical information engineering from the Jiangsu University of Science and Technology, Zhenjiang, China, in 2011, and the Ph.D. degree in information and communication engineering from Harbin Engineering University, Harbin, in 2018. She is now an Assistant Professor with the School of Oceanology, Jiangsu University of Science and Technology. Her research interests include metamaterials and antenna designs.

Yifan Shen was born in Wuxi, Jiangsu Province, China, in 2000. She received her B.S. degree in electronic information science and technology from Ocean College, Jiangsu University of Science and Technology in 2019. She is currently a graduate student at Ocean College, Jiangsu University of Science and Technology. Her research focuses on the cross-application of microwave technology, especially microwave hyperthermia treatment, including antenna design and optimization, phased array systems, and adaptive beamforming algorithms.

Atef Z. Elsherbeni is a renowned expert in electromagnetism, currently a professor at the Colorado School of Mines, and an IEEE Fellow and ACES Fellow. He received his Ph.D. in electrical engineering from the University of Manitoba in 1987 and subsequently taught at the University of Mississippi, where he held several academic and administrative positions. Elsherbeni's research has focused on computational electromagnetics, particularly in the application of finite-difference time-domain (FDTD) and finite-element methods (FEM). He has published a large number of academic papers and has given keynote speeches at several international conferences to share his research results and experience.

Yunlong Mao was born in Taizhou, Jiangsu, in 1989. He received the B.S. degree in electrical information engineering from the Jiangsu University of Science and Technology, Zhenjiang, China, in 2011, and the Ph.D. degree in information and communication engineering from Harbin Engineering University, Harbin, in 2018. He is now an Assistant Professor with the School of Oceanology, Jiangsu University of Science and Technology. His research interests include antennas and finite-difference time-domain method.

Cheng Lyu received her Bachelor's degree from Harbin Institute of Technology (HIT) in 2014 and earned his Doctor of Engineering degree in Information and Communication Engineering from Harbin Engineering University (HEU) in 2023. She currently serves as a Professor at Heilongjiang Agricultural Engineering Vocational College. Her research focuses on the intersection of microwave technology, particularly microwave thermotherapy for breast cancer, where she investigates non-invasive treatment systems. In the field of wireless communications, her expertise encompasses antenna design and optimization, phased array systems, and adaptive beamforming algorithms. Her work aims to advance both therapeutic technologiesand enhance the performance of intelligent antenna arrays for breast cancer hyperthermia therapy systems, bridging engineering innovation with potential clinical impact.